



A Multi-telescope Campaign on FRB 121102: Implications for the FRB Population

C. J. Law¹, M. W. Abruzzo², C. G. Bassa³, G. C. Bower⁴, S. Burke-Spolaor^{5,6,7}, B. J. Butler⁵, T. Cantwell⁸, S. H. Carey⁹, S. Chatterjee¹⁰, J. M. Cordes¹⁰, P. Demorest⁵, J. Dowell¹¹, R. Fender¹², K. Gourdji¹³, K. Grainge⁸, J. W. T. Hessels^{3,13}, J. Hickish^{1,9}, V. M. Kaspi¹⁴, T. J. W. Lazio¹⁵, M. A. McLaughlin^{6,7}, D. Michilli^{3,13}, K. Mooley¹², Y. C. Perrott⁹, S. M. Ransom¹⁶, N. Razavi-Ghods⁹, M. Rupen¹⁷, A. Scaife⁸, P. Scott⁹, P. Scholz¹⁷, A. Seymour¹⁸, L. G. Spitler¹⁹, K. Stovall^{5,11}, S. P. Tendulkar¹⁴, D. Titterton⁹, R. S. Wharton¹⁰, and P. K. G. Williams²⁰

¹ Department of Astronomy and Radio Astronomy Lab, University of California, Berkeley, CA 94720, USA

² Haverford College, 370 Lancaster Ave, Haverford, PA 19041, USA

³ ASTRON, The Netherlands Institute for Radio Astronomy, Postbus 2, NL-7990 AA, Dwingeloo, The Netherlands

⁴ Academia Sinica Institute of Astronomy and Astrophysics, 645 N. A'ohoku Place, Hilo, HI 96720, USA

⁵ National Radio Astronomy Observatory, Socorro, NM 87801, USA

⁶ Department of Physics and Astronomy, West Virginia University, Morgantown, WV 26506, USA

⁷ Center for Gravitational Waves and Cosmology, West Virginia University, Chestnut Ridge Research Building, Morgantown, WV 26505, USA

⁸ Jodrell Bank Centre for Astrophysics, Alan Turing Building, School of Physics & Astronomy, The University of Manchester, Oxford Road, Manchester M13 9PL, UK

⁹ Astrophysics Group, Cavendish Laboratory, 19 J. J. Thomson Avenue, Cambridge CB3 0HE, UK

¹⁰ Cornell Center for Astrophysics and Planetary Science and Department of Astronomy, Cornell University, Ithaca, NY 14853, USA

¹¹ Department of Physics and Astronomy, University of New Mexico, Albuquerque, NM 87131, USA

¹² Centre for Astrophysical Surveys, University of Oxford, Denys Wilkinson Building, Keble Road, Oxford OX1 3RH, UK

¹³ Anton Pannekoek Institute for Astronomy, University of Amsterdam, Science Park 904, 1098 XH Amsterdam, The Netherlands

¹⁴ Department of Physics and McGill Space Institute, McGill University, 3600 University St., Montreal, QC H3A 2T8, Canada

¹⁵ Jet Propulsion Laboratory, California Institute of Technology, Pasadena, CA 91109, USA

¹⁶ National Radio Astronomy Observatory, Charlottesville, VA 22903, USA

¹⁷ National Research Council of Canada, Herzberg Astronomy and Astrophysics, Dominion Radio Astrophysical Observatory, P.O. Box 248, Penticton, BC V2A 6J9, Canada

¹⁸ Arecibo Observatory, HC3 Box 53995, Arecibo, PR 00612, USA

¹⁹ Max-Planck-Institut für Radioastronomie, Auf dem Hügel 69, D-53121 Bonn, Germany

²⁰ Harvard-Smithsonian Center for Astrophysics, Cambridge, MA, USA

Received 2017 May 21; revised 2017 September 28; accepted 2017 October 10; published 2017 November 20

Abstract

We present results of the coordinated observing campaign that made the first subarcsecond localization of a fast radio burst, FRB 121102. During this campaign, we made the first simultaneous detection of an FRB burst using multiple telescopes: the VLA at 3 GHz and the Arecibo Observatory at 1.4 GHz. Of the nine bursts detected by the Very Large Array at 3 GHz, four had simultaneous observing coverage at other observatories at frequencies from 70 MHz to 15 GHz. The one multi-observatory detection and three non-detections of bursts seen at 3 GHz confirm earlier results showing that burst spectra are not well modeled by a power law. We find that burst spectra are characterized by a ~ 500 MHz envelope and apparent radio energy as high as 10^{40} erg. We measure significant changes in the apparent dispersion between bursts that can be attributed to frequency-dependent profiles or some other intrinsic burst structure that adds a systematic error to the estimate of dispersion measure by up to 1%. We use FRB 121102 as a prototype of the FRB class to estimate a volumetric birth rate of FRB sources $R_{\text{FRB}} \approx 5 \times 10^{-5}/N_r \text{ Mpc}^{-3} \text{ yr}^{-1}$, where N_r is the number of bursts per source over its lifetime. This rate is broadly consistent with models of FRBs from young pulsars or magnetars born in superluminous supernovae or long gamma-ray bursts if the typical FRB repeats on the order of thousands of times during its lifetime.

Key words: radio continuum: stars – stars: neutron – supernovae: general – techniques: interferometric

1. Introduction

Fast radio bursts (FRBs) were discovered ten years ago with the detection of a millisecond-duration radio transient with an anomalously high dispersion measure (DM; Lorimer et al. 2007). The large DMs imply that FRBs originate outside of our Galaxy, potentially at cosmological distances, and are orders of magnitude more luminous than pulses from Galactic pulsars (Thornton et al. 2013). There are now 23 FRBs publicly known²¹ with DMs as high as 1600 pc cm^{-3} and temporal widths of order milliseconds. Both their energetics and distance have inspired a wide variety of models and astrophysical applications (e.g., Kulkarni et al. 2014; McQuinn 2014; Fuller & Ott 2015; Connor et al. 2016b; Cordes & Wasserman 2016;

Popov & Pshirkov 2016). However, that potential was limited by the lack of a definitive association of an FRB to an extragalactic host.

This paper is part of a series based on the first localization of an FRB and its unambiguous association to an extragalactic host (Chatterjee et al. 2017; Marcote et al. 2017; Tendulkar et al. 2017). FRB 121102, also known as the “repeating FRB,” was discovered (Spitler et al. 2014) in data acquired in 2012 as part of the PALFA survey of the Arecibo Observatory (Cordes et al. 2006; Lazarus et al. 2015). In mid-2015, new Arecibo observations revealed a series of bursts at a similar DM and sky position that rules out cataclysmic models for this source (Spitler et al. 2016). The typical DM measured by early Arecibo observations was 559 pc cm^{-3} (Scholz et al. 2016), although somewhat higher values have been seen in more

²¹ See <http://frbcat.org> (Petroff et al. 2016).

recent observations (560.5 pc cm^{-3} ; J. W. T. Hessels et al. 2017, in preparation).

Beginning in 2016 August (MJD 57623), we made the first of nine detections of FRB 121102 with the Karl G. Jansky Very Large Array (VLA; Chatterjee et al. 2017) and localized it with a precision of $0''.1$. Deep optical observations with the Gemini Observatory associated the FRB with a host galaxy at $z = 0.193$ (Tendulkar et al. 2017) and the European VLBI Network detected four more bursts to localize the source with a precision of $0''.01$, four orders of magnitude better than any other FRB (precision of $\sim 40 \text{ pc}$ in linear distance; Marcote et al. 2017). The lookback and luminosity distances for FRB 121102 are 746 and 972 Mpc, respectively, assuming a concordance cosmology with parameters given by Planck Collaboration et al. (2016). If FRB 121102 is representative of all FRBs, then we should expect them to be useful as probes of the intergalactic medium and their host galaxies (Macquart & Johnston 2015). Thus, the confirmation of a cosmological distance for FRB 121102 has begun to fulfil the promise implied by the first FRB detection.

Many new models for the origin of FRBs have been developed in response to the localization of FRB 121102 (Beloborodov 2017; Dokuchaev & Eroshenko 2017; Kashiyama & Murase 2017; Metzger et al. 2017; Thompson 2017; Zhang 2017). The association of FRB 121102 with a compact, persistent radio source is consistent with bursts coming from a young magnetar that powers a luminous pulsar wind nebula (Kashiyama & Murase 2017). At the same time, FRB 121102 is found in a low-metallicity dwarf galaxy (Tendulkar et al. 2017), which was not predicted by origin models that scale with stellar mass or star formation (Nicholl et al. 2017). These galaxies are the preferred environment for long GRBs and hydrogen-poor superluminous supernovae (LGRBs and SLSN-I, respectively), which have been suggested are signatures of magnetar birth (Modjaz et al. 2008; Lunnan et al. 2014).

This paper presents an analysis of the spectral properties of VLA bursts implied by detections and nondetections during observation at Arecibo, Effelsberg, the first station of the Long Wavelength Array (LWA1; Ellingson et al. 2013), and the Arcminute Microkelvin Imager Large Array (AMI-LA; Zwart et al. 2008). This includes the first simultaneous detection of an FRB at two observatories, between the VLA and Arecibo. If we assume that FRB 121102 is representative of all FRBs, we can use it to constrain the physical processes at play in the overall FRB population. The repetition of FRB 121102 also has strong implications for calculations of their rate of occurrence (Connor et al. 2016a) and comparison to other classes of transient, such as superluminous supernovae (Tendulkar et al. 2017).

In Section 2, we describe the multi-telescope observing campaign and a refined analysis of the nine VLA bursts. Section 3 presents the first spectrum of an FRB simultaneously detected at multiple telescopes, confirming that burst spectra cannot be modeled with a single spectral index. We then model the dynamic spectra to characterize the burst spectra, energies, and dispersion properties. Section 4 discusses the properties of FRB 121102 bursts and their impact on inferences about the birth rate of FRB sources and strategies to find and/or localize new FRBs.

2. Observations

The data presented here were obtained from multiple programs and telescopes with the goal of interferometrically localizing FRB 121102 with the VLA. We coordinated observing between the VLA, Arecibo, Effelsberg, LWA1, and AMI-LA telescopes, as shown in Figure 1 and Table 1. Table 2 summarizes the instrument configurations for all observations presented here.

Computational (Jupyter) notebooks to reproduce the transient detection, localization, and analysis presented here can be found at <https://github.com/caseyjlaw/FRB121102> and at the Harvard Dataverse [doi:10.7910/DVN/ZKESD4]. Time cut-out visibility data and calibration products are available at the Harvard Dataverse [doi:10.7910/DVN/TLDKXG]. Original VLA visibility data are available under NRAO program codes 16A-459 and 16A-496 and can be downloaded at <http://archive.nrao.edu>.

2.1. VLA

The FRB 121102 observing campaign started in 2015 November with a 10 hr campaign ($\sim 1 \text{ hr}$ per session) observed at 1.4 GHz in the compact D configuration. In 2016 April through May, we conducted a 40 hr campaign ($\sim 2 \text{ hr}$ per session) at 3 GHz in the C and CnB configurations in coordination with Arecibo (Scholz et al. 2016). We concluded with a 40 hr, coordinated campaign ($\sim 2 \text{ hr}$ per session) from 2016 August through September in the B configuration and during the move to the most extended A configuration. In the late 2016 campaign, the first 34 hr of VLA observations were made at 3 GHz, while the last 6 hr were observed at 6 GHz. These observing session times are inclusive of calibration and overhead, which typically amounts to 15% of the total observing time.

All VLA fast-sampled data were observed with 5 ms sampling, 256 frequency channels, and dual-circular polarization (Law et al. 2015). As shown in Table 2, the L (1.4 GHz), S (3 GHz), and C (6 GHz) bands were used with channel resolutions that kept dispersion smearing well below the temporal resolution. All detections were made in the 3 GHz data, which were recorded in eight spectral windows with 32 channels each and had a sensitivity of 4 mJy in 5 ms (1σ).

Observations in August and September were searched by a prototype version of *realfast*,²² a real-time, fast imaging transient search system. The current prototype runs on CPU-based hardware that is normally dedicated to the VLA correlator; for this experiment, it runs the transient search pipeline software called *rtpipe* (Law 2017). Images were formed for each integration with DMs of 0, 546, 556.9, 560, and 565 pc cm^{-3} and a time resampling grid of 5, 10, 20, 40, and 80 ms. This DM grid was chosen to maintain 90% sensitivity to the nominal DM range of 540–570 pc cm^{-3} . Gain calibration was made from observations of J0555+3948 by an automated system (telcal), which uses phase-only calibration. A flux scale was calculated for each spectral window from an observation of 3C48 and applied to all burst spectra, and had an accuracy of about 10%.

Burst detections and localizations were made within 5–10 hr of data being recorded. The transient search starts when data are recorded and proceeds at anywhere from 1 to 30 times

²² See <http://realfast.io>.

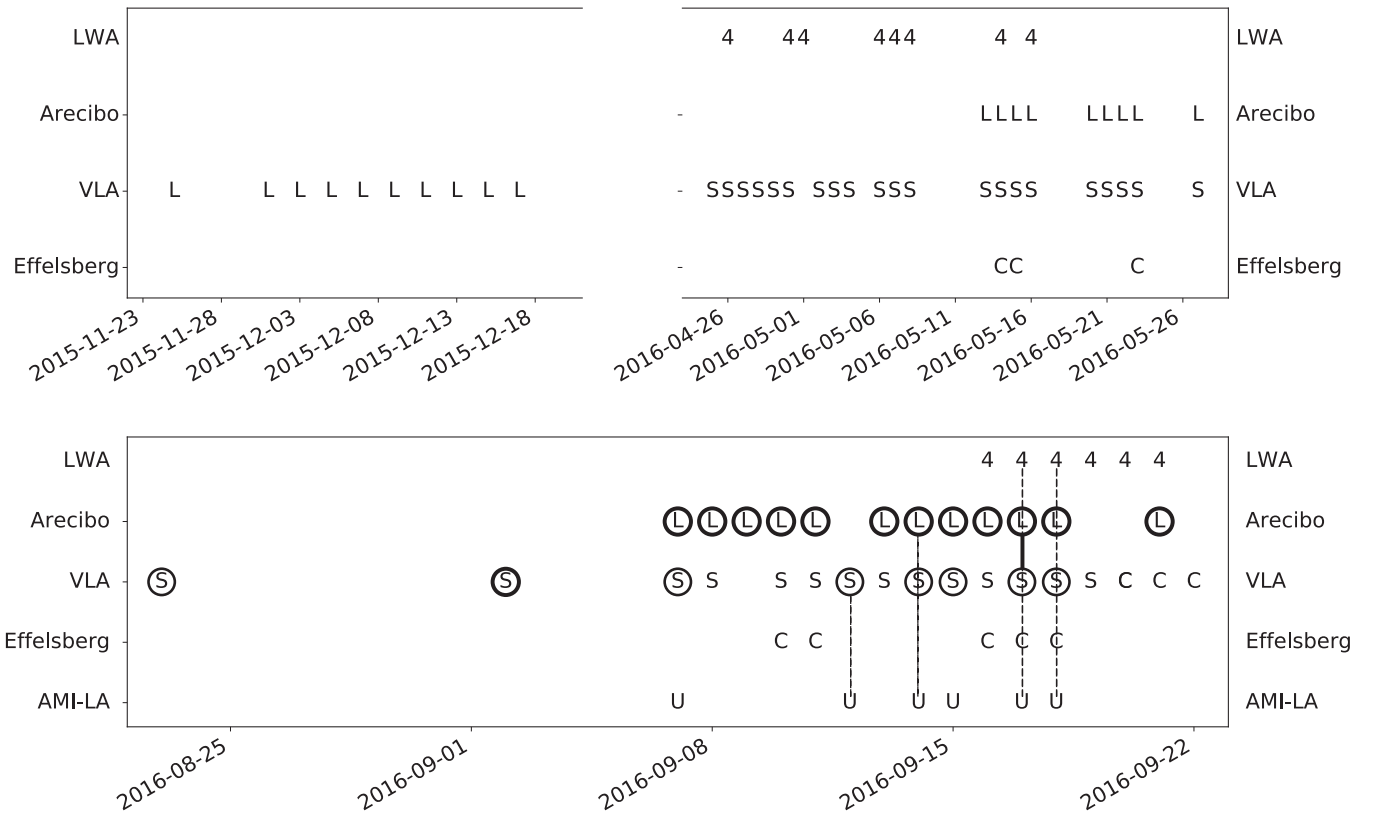


Figure 1. Top and bottom panels summarize the observations and detections of FRB 121102 in the 2015 and 2016 campaigns. Circles highlight observations that detected bursts from FRB 121102 with multiple burst detections indicated with a heavy line. The black dashed lines show the VLA burst detections with simultaneous coverage at other telescopes and the solid line shows the simultaneous burst detection. Circled observations with no line indicate bursts that did not have simultaneous observing coverage at the VLA. Days with observations are indicated with radio band designations 4, L, S, C, U referring to radio frequencies of 70 MHz, 1.4, 3, 4.85, and 15 GHz, respectively.

slower than real-time, depending on the number of compute nodes available, array configuration, and number of DMs searched. For each trial DM, integration, and timescale, we form an image and calculate the signal-to-noise ratio (S/N) for the peak pixel in the dirty image. We empirically identified S/N thresholds of 6.4 and 7.4 as useful to capture data quality statistics and candidates for inspection, respectively. The higher threshold is relatively unlikely to be triggered by thermal noise in this configuration, so *realfast* generates a more detailed (and computationally intensive) candidate visualization that includes an image and spectrum. All visibilities are recorded so detailed analysis, including improved calibration and localization, can be conducted offline.

2.2. Arecibo

Arecibo observed with the L-wide receiver using the PUPPI pulsar backend (DuPlain et al. 2008; Ford et al. 2010). The observational frequency range was 1.15 to 1.73 GHz and frequency resolution was 1.5625 MHz, which has a typical sensitivity of 2 mJy in 2 ms (1σ). We recorded intensities of the each of the two orthogonal linear polarization signals and their cross product. Full Stokes polarization intensity spectra can then be generated with a time resolution of $10.24 \mu\text{s}$. Each frequency channel was coherently dedispersed to 557 pc cm^{-3} , significantly reducing intra-channel dispersion smearing. The full width at half maximum (FWHM) beam size at band center is $3/3$.

In total, 11 Arecibo observations had some simultaneous coverage with the VLA. All of these observations were

conducted after the VLA localization, so they were pointing directly at FRB 121102. Three of those Arecibo observations detected no burst coincident with the VLA bursts, while one Arecibo observation detected a burst coincident with the VLA burst. Overall, there were many more bursts detected at Arecibo than with the VLA, including some Arecibo bursts with simultaneous VLA upper limits. A more detailed analysis of those bursts will be presented elsewhere (D. Michilli et al. 2017, in preparation).

2.3. Effelsberg

Effelsberg observations were conducted with the S60mm receiver and recorded total intensity spectra with the PFFTS backend in pulsar search mode with a time resolution of $65.5 \mu\text{s}$. The receiver has a system equivalent flux density of 18 Jy and a FWHM beam size of $2/4$ at 4.85 GHz.

Five Effelsberg observations were made pointing at the known location of FRB 121102 and had some simultaneous coverage with the VLA. Two of these observations were simultaneous with VLA bursts, but made no detection. The nominal receiver bandwidth is from 4.6 to 5.1 GHz, but a configuration error reduced effective bandwidth to 100 MHz centered at 4.85 GHz for both of these observations during VLA bursts. The sensitivity in these observations was about 28 mJy in 2 ms (1σ), which is two times worse than the full-bandwidth value. No burst was detected in either of the two observations that were simultaneous with a VLA burst detection.

Table 1
VLA Observations of FRB 121102

MJD	Date/time (ymd/hms)	Duration (minute)	Freq. (GHz)	Bursts
57351	2015 Nov 25/03:25:29	60	1.4	0
57357	2015 Dec 01/05:31:31	60	1.4	0
57359	2015 Dec 03/02:53:57	60	1.4	0
57361	2015 Dec 05/04:45:44	60	1.4	0
57363	2015 Dec 07/04:37:50	60	1.4	0
57365	2015 Dec 09/09:29:25	60	1.4	0
57367	2015 Dec 11/09:22:27	60	1.4	0
57369	2015 Dec 13/09:13:07	60	1.4	0
57371	2015 Dec 15/09:06:16	60	1.4	0
57373	2015 Dec 17/08:57:51	60	1.4	0
57503	2016 Apr 25/23:21:39	240	3	0
57504	2016 Apr 26/23:14:31	120	3	0
57505	2016 Apr 27/23:26:09	120	3	0
57506	2016 Apr 28/22:41:31	120	3	0
57507	2016 Apr 29/22:37:34	120	3	0
57508	2016 Apr 30/19:14:46	60	3	0
57510	2016 May 02/23:14:18	60	3	0
57511	2016 May 03/22:53:26	60	3	0
57514	2016 May 06/18:25:12	60	3	0
57515	2016 May 07/19:34:13	60	3	0
57516	2016 May 08/19:30:20	60	3	0
57521	2016 May 13/17:12:48	135	3	0
57522	2016 May 14/17:14:11	135	3	0
57523	2016 May 15/17:15:26	135	3	0
57524	2016 May 16/16:59:52	135	3	0
57528	2016 May 20/16:45:46	135	3	0
57529	2016 May 21/16:44:06	135	3	0
57530	2016 May 22/16:43:53	135	3	0
57531	2016 May 23/16:44:11	135	3	0
57535	2016 May 27/16:29:34	135	3	0
57623	2016 Aug 23/17:26:28	54	3	1
57633	2016 Sep 02/15:52:17	54	3	2
57638	2016 Sep 07/10:14:50	120	3	1
57639	2016 Sep 08/10:14:40	120	3	0
57641	2016 Sep 10/09:59:36	120	3	0
57642	2016 Sep 11/09:59:49	120	3	0
57643	2016 Sep 12/09:15:19	120	3	1 ^a
57644	2016 Sep 13/09:23:59	120	3	0
57645	2016 Sep 14/09:20:23	120	3	1 ^{a,b}
57646	2016 Sep 15/09:16:29	120	3	1
57647	2016 Sep 16/09:11:23	120	3	0
57648	2016 Sep 17/08:59:20	120	3	1 ^{a,c,d,e}
57649	2016 Sep 18/08:59:27	120	3	1 ^{a,b,d,e}
57650	2016 Sep 19/08:44:32	120	3	0
57651	2016 Sep 20/08:44:33	120	3	0
57651	2016 Sep 20/17:19:03	120	6	0
57652	2016 Sep 21/09:13:57	120	6	0
57653	2016 Sep 22/09:12:24	120	6	0

Notes. Times are in UT. Duration includes overhead, which is typically 15%. Frequency is the approximate center of the bandwidth.

^a AMI-LA nondetection at 15 GHz.

^b Arecibo nondetection at 1.4 GHz.

^c Arecibo detection at 1.4 GHz.

^d Effelsberg nondetection at 4.85 GHz.

^e LWA1 nondetection near 62 and 78 MHz.

2.4. LWA1

Beginning in 2016 April, VLA observations of FRB 121102 were simultaneously observed with LWA1 when possible. The

LWA1 observations were automatically scheduled through the Heuristic Automation for LWA1 (HAL) system. This system receives messages via the internet that signal the start of a VLA observation. If the source is visible and there are no high priority LWA1 observations scheduled, the HAL system automatically generates an observing schedule, re-configures the telescope, and alerts the observatory staff of the change. The time delay from HAL receiving a message to starting an observation is typically one to two minutes.

The LWA1 observations consisted of a single phased-array beam centered on the location of FRB 121102 with two 4096-channel spectral windows spanning frequencies from 52.2–71.8 MHz and 68.2–87.8 MHz. The sample time of 160 ms was set to be equal to the dispersion smearing across a single channel at 50 MHz for $DM \approx 560 \text{ pc cm}^{-3}$.

Two of the VLA detected pulses, on MJD 57648 and 57649, were not detected during simultaneous observations with LWA1. We used the modeled LWA1 antenna sensitivity as a function of zenith angle to estimate an system equivalent flux density of 9.5 and 8.7 kJy for the two bursts, respectively. The data were de-dispersed into time series with DMs ranging from 500 to 600 pc cm^{-3} using a step size of 1.0 pc cm^{-3} . Each spectral window was searched using PRESTO (Ransom 2001) with a boxcar matched-filtering width from the native time resolution up to 48 s. We also visually inspected the dedispersed time series for the DM range 557 to 560 pc cm^{-3} .

No dispersed pulses were found with significance greater than 10σ , equivalent to a flux density limit of $\sim 60 \text{ Jy}$ for a width of 160 ms. The system equivalent flux density does not change much between the two windows. The effective sensitivity to a typical 2 ms pulse width is 4.8 kJy.

2.5. AMI-LA

We observed FRB 121102 with AMI-LA for 3 hr each on six epochs starting at MJDs 57638, 57643, 57645, 57646, 57648, and 57649 (see Figure 1). Observations were made with the new digital correlator having 4096 channels across a 5 GHz bandwidth between 13 and 18 GHz with a 1 s integration time. The phase calibrator, J0518+3306, was observed for 1.5 minutes; this observation was repeated every 12 minutes. The AMI-LA data were binned to eight 0.625 GHz channels and processed (interference excision and calibration) with a fully automated pipeline, AMI-REDUCE (e.g., Perrott et al. 2013). Daily measurements of 3C48 and 3C286 were used for the absolute flux calibration, which is good to about 10%.

We inspected the calibrated visibilities, and did not find any signal above 30 mJy in the 1 s samples at and in the vicinity of the detected bursts. This corresponds to a sensitivity of 15 Jy for an assumed pulse width of 2 ms. Concatenating and imaging the 12 hr of calibrated data with the CASA tasks *concat* and *clean* also does not yield any significant detection at the FRB location. Although the statistical 3σ upper limit is 60 μJy , extended mJy-level sources in the field cause sidelobe confusion (the AMI-LA angular resolution is $\sim 30''$), and the actual upper limit is larger. We introduced artificial point sources at the FRB location using the CASA *sm* tool, and found that these sources can be recovered at 3σ as long as their peak flux densities are more than $\sim 100 \mu\text{Jy}$. Hence, we place an upper limit of $100 \pm 10 \mu\text{Jy}$ on any quiescent or possible radio flaring on \sim days timescales from the FRB. This limit is

Table 2
Observing Configurations

Telescope	Freq. Center (GHz)	Freq. Bandwidth (MHz)	Freq. Resolution (MHz)	Time resolution (ms)	DM smearing ^a (ms)	Sensitivity (1 σ ; Jy ms)
LWA	0.062/0.078 ^b	19.6	0.0048	160	83/43	9600
Arecibo	1.44	580	1.5625	0.01024	0.0 ^c	0.004
VLA	1.4	256	1	5	1.7	0.050
VLA	3.0	1024	4	5	0.7	0.020
VLA	6.0	2048	8	5	0.2	0.013
Effelsberg	4.85	500 ^d	3.4	0.0655	0.032	0.056
AMI-LA	15	5000	625	1e3	0.0	30

Notes.

^a DM smearing calculated for nominal FRB 121102 DM of 560.5 pc cm^{-3} at the center frequency.

^b LWA1 observed with two independent bands with identical configurations and sensitivities.

^c Arecibo data are coherently dedispersed to 560.5 pc cm^{-3} , so DM smearing is effectively eliminated.

^d Effelsberg recorded 500 MHz of bandwidth, but a filter reduced the effective bandwidth to 100 MHz for the two days with coincident VLA FRB detections (MJD 57648 and 57649).

similar to the flux density measured by the VLA at 12 GHz for the persistent source (Chatterjee et al. 2017).

3. Results

Here we present the analysis of the VLA bursts detected toward FRB 121102 with a focus on constraints from coordinated radio observations. In total, nine bursts were detected by the VLA. Three of those bursts had observing coverage by other telescopes, yet were not detected. One of the VLA bursts was detected by another telescope, Arecibo. In Section 3.1, we describe the spectral properties implied by multi-frequency detections and nondetections of VLA bursts at 3 GHz. Section 3.2 presents a deeper study of the VLA bursts alone, including a spectrotemporal modeling of the bursts, their energies, and their temporal distribution.

3.1. Multi-observatory Burst Spectrum

Figure 2 shows a dynamic spectrum for the first FRB burst to be detected simultaneously at two telescopes. This burst, on MJD 57648, was detected both by the VLA and Arecibo while upper limits were measured by simultaneous observations at the other three telescopes. In total, four of the VLA bursts had simultaneous observing coverage with either Arecibo, Effelsberg, LWA1, or AMI-LA. Two of the VLA bursts had simultaneous observing coverage by all four observatories, including the burst detected by Arecibo.

To generate the multi-telescope dynamic spectrum, the VLA and Arecibo data were resampled to the same temporal grid relative to the start time of the Arecibo data. We corrected for barycentric and DM offsets by assuming a DM of 560.5 pc cm^{-3} (J. W. T. Hessels et al. 2017, in preparation). The dispersion delay was 189 and 734 ms from infinite frequency to the top of the VLA and Arecibo bands, respectively. An error in the DM of 1 pc cm^{-3} corresponds to a delay time correction error of 0.3 and 1.4 ms for the VLA and Arecibo bands, respectively. We used PRESTO to calculate a relative barycentric time correction of 3.8 ms between the VLA and Arecibo at the time of observation.

The regridded dynamic spectrum has an apparent DM error that is evident both as a frequency-dependent time drift within the Arecibo observation and as an offset between the Arecibo and VLA bursts. Both of these drifts are consistent with an apparent DM of $\sim 565 \text{ pc cm}^{-3}$. More refined modeling of the

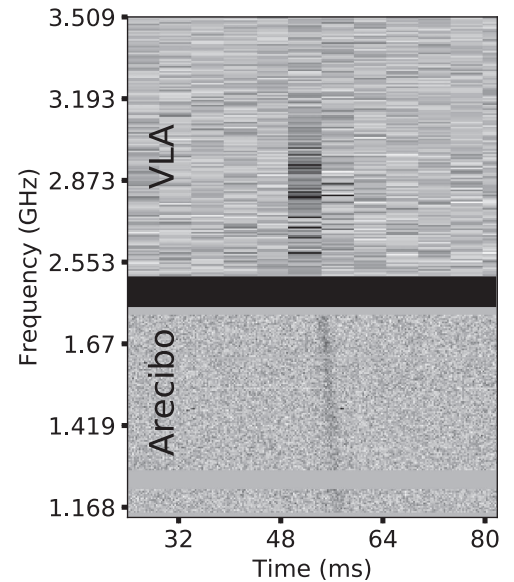


Figure 2. Composite dynamic spectrum for the burst from FRB 121102 on MJD 57648 with data from the VLA and Arecibo observatories. The time axis is centered on the burst and starts at MJD 57648.437788874842, corrected to the barycenter and infinite frequency assuming $\text{DM} = 560.5 \text{ pc cm}^{-3}$. The thick black line separates data from the VLA (2.5–3.5 GHz) and Arecibo (1.1 to 1.8 GHz) and flagged data are gray. For clarity, the VLA and Arecibo data are independently normalized to units of S/N per pixel; Arecibo is five times more sensitive than the VLA.

VLA dynamic spectrum alone (Section 3.2.1 and Table 3) is consistent with this higher DM value.

Figure 3 shows coarse spectra built from integrated flux densities measured (or limited) for the three VLA bursts with observing coverage by Arecibo or Effelsberg. The burst on MJD 57648 was detected with VLA and Arecibo with significances of 25σ and 39σ , which corresponds to peak flux densities in 5 ms of $111 \pm 5 \text{ mJy}$ and $14 \pm 0.4 \text{ mJy}$ at 3 and 1.4 GHz, respectively. The VLA observations under-resolve the pulses in time, so to compare these values, we assume a typical pulse width of 2 ms. Under this assumption, the VLA and Arecibo integrated flux densities are 278 ± 13 and $57 \pm 2 \text{ mJy}$ at 3 and 1.4 GHz, respectively. Assuming a power-law flux density model ($S_\nu \propto \nu^\alpha$), we find a spectral index $\alpha = 2.1$. This is inconsistent with the spectral index limit

Table 3
Properties of FRB 121102 Bursts Seen by VLA at 3 GHz

Time		Observed Properties			Modeled Properties					
Calendar day (2016)	Burst time (MJD)	S/N (image)	$S_{I,5\text{ ms}}$ (mJy)	S_V (mJy)	DM (pc cm ⁻³)	W (ms)	$S_{I,\text{peak}}$ (mJy)	Center (GHz)	FWHM (MHz)	E_{int} (10 ³⁸ erg)
Aug 23	57623.74402686	38	194	+3	567 ± 2	2.0 ± 0.2	690	2.8	290	12
Sep 2	57633.67986367	179	1500	-35	568.2 ± 0.2	2.05 ± 0.02	3340	3.2	510	98
Sep 2 ^c	57633.69515938	15	69	+2	562 ⁺⁴ ₋₆	2.5 ^{+0.9} _{-0.6}	>430	<2.5	<290	7
Sep 7	57638.49937435	12	55	+5	567 ⁺⁷ ₋₉	1.3 ^{+1.4} _{-0.8}	130	3.1	420	3
Sep 12 ^a	57643.45730263	100	508	-5	565.6 ^{+0.6} _{-0.5}	1.9 ± 0.1	1170	2.8	510	34
Sep 14 ^a	57645.42958602	13	64	+3	563 ⁺⁵ ₋₄	1.1 ± 0.7	170	2.8	380	4
Sep 15 ^c	57646.46600650	20	87	+1	569 ± 5	2.5 ^{+0.9} _{-1.4}	>420	<2.5	<430	10
Sep 17 ^{a,b}	57648.43691490	25	111	+9	564 ± 2	1.4 ^{+0.3} _{-0.4}	260	2.8	470	7
Sep 18 ^a	57649.45175697	36	167	+1	567 ± 2	2.1 ± 0.5	290	3.0	690	12

Notes. Burst times are topocentric at the VLA at 3.5 GHz. S_V is the measured circular polarization of the burst, which is dominated by systematic effects. All error ranges represent 68% confidence intervals.

^a Simultaneously observed with either Arecibo, Effelsberg, LWA1, or AMI-LA.

^b Detected with Arecibo.

^c Best-fit Gaussian is not centered in 3 GHz band, so spectral parameters are limits.

implied by the Effelsberg nondetection at 4.85 GHz ($\alpha < -1.4$ for a 2 ms burst and 5σ limit).

Overall, the burst detections and nondetections show that burst spectra are not well described by a power-law model. Two Arecibo nondetections and two Effelsberg nondetections of VLA bursts place mutually inconsistent lower and upper limits on the spectral index. The Arecibo and Effelsberg upper limits at 1.4 and 4.85 GHz, respectively, limit all burst spectral indices $\alpha_{1.4/3} > +4.9$ and $\alpha_{3/4.85} < -2.3$. These are consistent with limits from the LWA1 and AMI-LA, which require $\alpha_{0.07/3} > -2.4$ and $\alpha_{3/15} < 1.5$ for bursts on MJD 57643 and 57649 (the brightest VLA bursts with observing coverage), respectively. The strictest limits on $\alpha_{1.4/3}$ and $\alpha_{3/4.85}$ are both derived from the burst on MJD 57649, which shows that a power-law model is inappropriate even for a single burst.

3.2. VLA Bursts

3.2.1. Spectrotemporal Modeling

This paper refines the analysis of the nine VLA radio burst spectra described in Chatterjee et al. (2017) in a few ways. We use a better calibration scheme and have optimized the detection significance over a fine grid of DM ($\Delta\text{DM} = 1 \text{ pc cm}^{-3}$). After calibration and flagging, the visibility phases were rotated to the best-fit location (R.A., decl. = 05^h31^m58^s.70, +33^d08^m52^s.5; Chatterjee et al. 2017) to extract a Stokes I spectrum that maximizes the image S/N for each burst.

Table 3 summarizes the spectrotemporal properties of all nine VLA bursts. Parameters such as integrated flux density, S/N, and Stokes V were measured from the burst properties integrated in frequency. The circular polarization fraction (Stokes V/I) was estimated as $(RR - LL)/(RR + LL) \approx 3\%$, which is comparable to the systematic error expected from beam squint at this location in the primary beam.²³ Given that systematic effects dominate the apparent circular polarization, this observation limits the fractional circular polarization to less than 3%.

²³ See EVLA memo #195 at https://library.nrao.edu/public/memos/evla/EVLAM_195.pdf.

Figure 4 shows that the Stokes I spectra are generally characterized by a broad, Gaussian shape with inter-channel modulation as high as 100%. Diffractive scintillation from the Milky Way has a typical bandwidth of 7 MHz at a reference frequency of 3 GHz along this line of sight (Cordes & Lazio 2002), which is similar to the channel size of 4 MHz. The burst energy is calculated from the flux density in 5 ms and integrating over the optimal Gaussian spectral model.

The dynamic radio spectra (time versus frequency) were modeled using a Markov chain Monte Carlo (MCMC) method. We used the Goodman and Weare affine invariant sampler (Goodman & Weare 2010) as implemented in *emcee* (Foreman-Mackey et al. 2013). The dynamic spectra were modeled prior to dispersion correction. The spectral structure was modeled as a broad Gaussian envelope as

$$G(\nu) = S_{I,\text{peak}} \exp\left[-\frac{1}{2}\left(\frac{\nu - \nu_0}{\sigma}\right)^2\right], \quad (1)$$

where $S_{I,\text{peak}}$ is the peak flux density in mJy per 5 ms integration, ν_0 is the Gaussian center frequency, and σ is its width. The arrival time was modeled with a cold plasma dispersion law with the arrival time in units of integrations of

$$i(\nu) = i0 + 4.1488 \times 10^{-3} \text{ DM}(\nu^{-2} - \nu_0^{-2})/(5\text{ms}), \quad (2)$$

where $i0$ is the arrival integration at the highest frequency and ν is in units of GHz. Finally, the pulses were assumed to have an intrinsically square temporal width (parameter W_{int}). These six parameters defined the intrinsic signal that was then distributed over a fixed time-frequency observing grid.

We use a log likelihood function $\ln \mathcal{L} = (-1/2) \sum_i (S_i - S_{i,\text{model}})^2 / \sigma_s^2$ where S_i refers to the measured and modeled flux density in a single pixel of the dynamic spectrum and $\sigma_s \approx 70 \mu\text{Jy}$ is the measured off-burst noise per 5 ms integration and 4 MHz channel. A flat prior was used over all ranges with valid data with the requirement that the integrated signal must have a detection significance higher than 8σ . The six-dimensional models were sampled with 100 chains taking 700 steps; we ignored the first 200 steps to properly sample the posterior distributions.

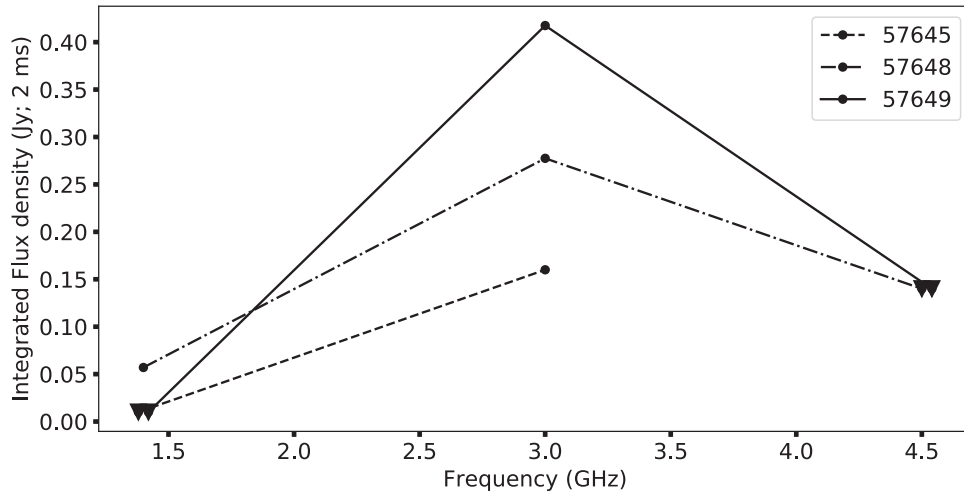


Figure 3. Broadband spectral measurements and limits for three bursts of FRB 121102 with observing coverage by Arecibo or Effelsberg. Upper limits assume a pulse width of 2 ms and a 5σ detection threshold. Measurements (dots) and limits (triangles) are shown for Arecibo, VLA, and Effelsberg at 1.4, 3, and 4.85 GHz, respectively; limits from LWA1 and AMI-LA are not visible on this scale. Errors in flux density are comparable to the symbol size and are not shown. Overlapping points are offset by tens of MHz in frequency for clarity.

The parameters for the best model of the dynamic spectrum are given in Table 3 and the resulting Gaussian model overlaid on Figure 4. Two of the best-fit Gaussians are centered at the boundary of the 3 GHz band, so parameter estimates are actually limits. The other seven best-fit models appear contained by the 1 GHz wide band ($>90\%$ of the modeled flux is within the 3 GHz band). In all cases, the typical burst spectrum has a FWHM of approximately 500 MHz. This confirms previous reports based on Arecibo and GBT data (Scholz et al. 2016; Spitler et al. 2016) with the wider (1 GHz) VLA bandwidth and extends this phenomenon to 3 GHz.

Our approach simultaneously models the spectral and temporal evolution of the burst. A typical FRB 121102 burst takes ~ 180 ms or 36 integrations to cross the observing band from 2.5 to 3.5 GHz. The effect of a finite pulse width is visible as the burst moves from one integration to the next, even for widths narrower than the integration time of 5 ms. Table 3 shows that the typical burst width is measured as 2 ± 0.5 ms (68% confidence interval); the intra-channel dispersion smearing ranges from 0.4 to 1.1 ms across this band. The brightest burst (on MJD 57633.68) is modeled with a temporal width of 2.05 ± 0.02 ms and its arrival time is measured with a precision of ~ 50 μ s. Note that these errors are only accurate to the degree that the model represents the data. One potential bias in the model is that we do not model scintillation effects or frequency-dependent temporal width.

While most bursts are modeled with well-defined parameter probability distributions, one burst is an outlier. Figure 5 shows the scatter plot matrix (Foreman-Mackey 2016) for the MCMC run on burst 57646. Two clusters of samples are identified for this burst: one narrow, low-DM and one wide, high-DM. This shows that the model is not appropriate for this burst and could indicate that the burst can be decomposed into two sub-bursts, as has been noted before for FRB 121102 (Scholz et al. 2016; Spitler et al. 2016).

3.2.2. Dispersion

The spectrotemporal modeling presented in Section 3.2.1 provides marginalized posterior distributions for burst DM and

pulse width. Figure 6 compares the 68% confidence intervals on the DM for all nine VLA bursts against detection time (top panel) and the modeled burst temporal width (bottom panel). The error-weighted mean burst DM is 567.8 ± 0.1 pc cm^{-3} , significantly larger than the long-term average of 560.5 pc cm^{-3} seen by Arecibo during this campaign. Furthermore, several of the 95% confidence intervals in DM are not consistent with this mean or each other, which suggests that we measure an apparent DM that is biased by some burst-specific property. The variation in DM observed by the VLA at 3 GHz is similar to that reported for Arecibo observations of FRB 121102 in Scholz et al. (2016) and Spitler et al. (2016).

The bottom panel of Figure 6 compares the DM to the modeled temporal width of the bursts. There is a weak correlation between burst width and apparent DM. A change in width of ~ 1 ms correlates with a change in apparent DM of approximately 5 pc cm^{-3} . It is not clear whether this correlation is driven by intrinsic structure or unmodeled effects, such as frequency-dependent temporal width. Future modeling could use a more complex (e.g., multi-component) model to distinguish between these possibilities.

3.2.3. Fine Spectral Structure

The spectral fits in Figure 4 have residuals that include single samples that deviate by many standard deviations, particularly in the bursts on MJDs 57623, 57633.6, and 57643. These do not appear to be caused by terrestrial interference. They are most likely spectral variations from diffractive Galactic scintillations that, as noted previously, have characteristic frequency widths slightly larger than the 4 MHz channel bandwidth. Scintillation variations are multiplicative and have a one-sided exponential probability distribution function that can yield occasional large-amplitude “scintles” that are several times the mean scintle amplitude of unity.

The spectral variations could in principle also include contributions from self-noise in the source but, to be significant, intrinsic fine structure in the burst would have to be on microsecond scales.

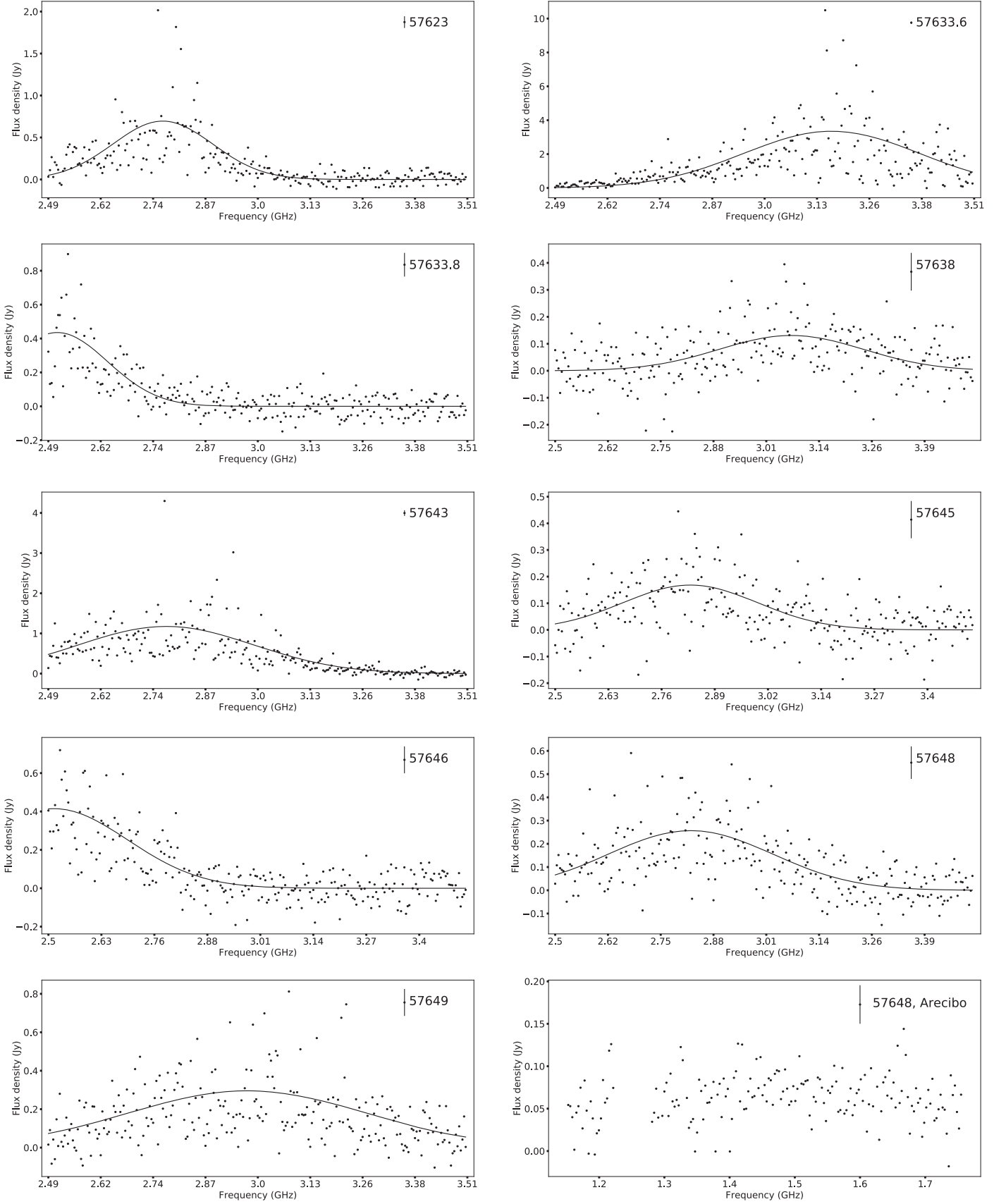


Figure 4. Ten panels show spectra for nine VLA bursts and one Arecibo burst (bottom right). The VLA spectra are drawn from flux-calibrated, dedispersed 5 ms integrations. The Arecibo spectrum is drawn from a 2.7 ms window with 3.125 MHz channels and the flux scale is estimated using the radiometer equation. The solid line shown with VLA spectra is a best-fit Gaussian model found through modeling; no comparable modeling is done for the Arecibo spectrum. The typical VLA flux density error per channel is 70 mJy, which is shown at the top right of each panel next to the MJD label.

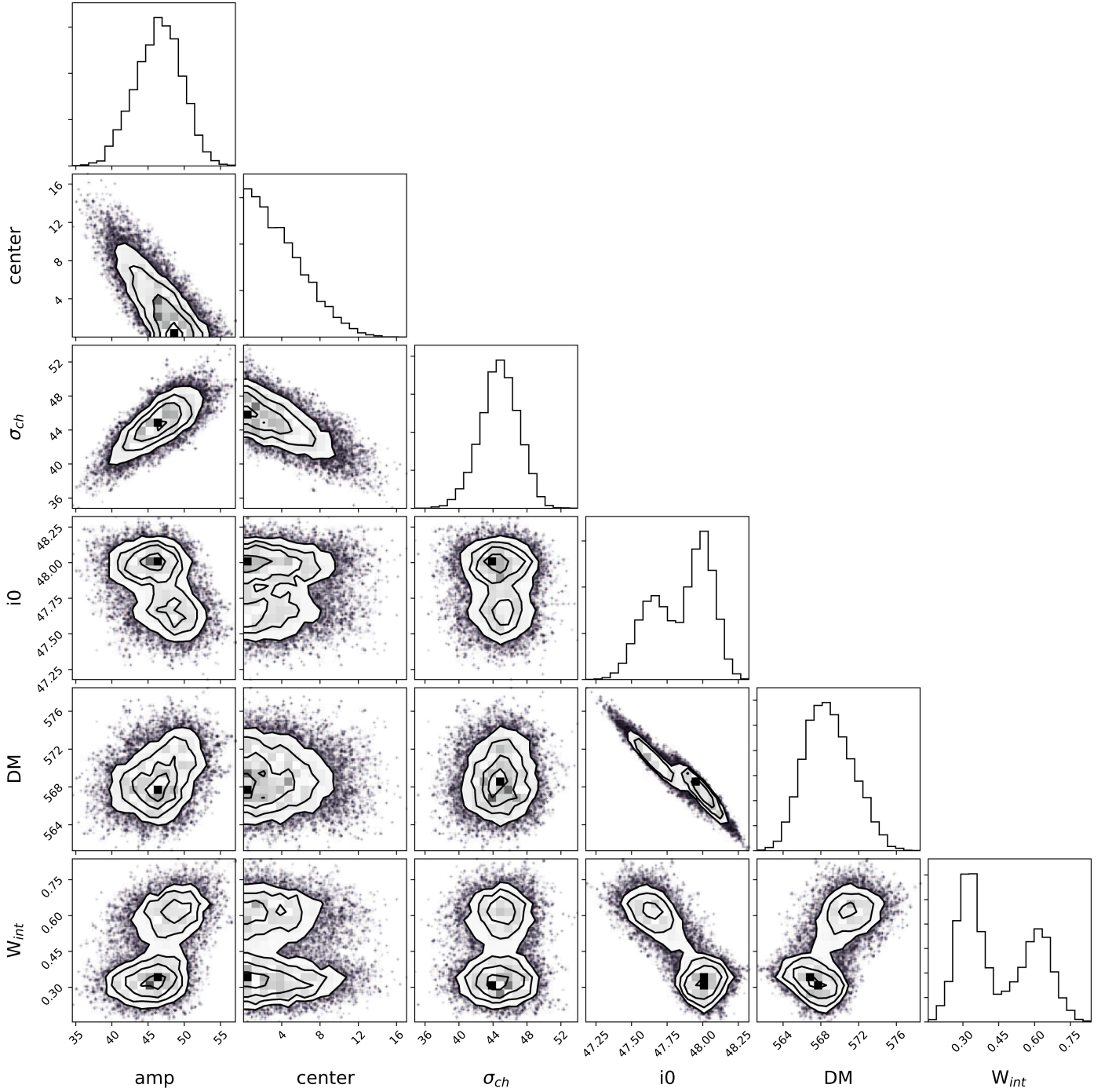


Figure 5. Scatterplot matrix showing the correlation of every pair of parameters in the MCMC run for burst 57646. The equivalent plots for the other bursts show normally distributed samples, but this burst shows significant structure in the samples. The parameters “amp,” “center,” and “ σ_{ch} ” refer to the Gaussian spectral shape, while “DM,” “ i_0 ,” and “ W_{int} ” refer to the temporal shape. The parameters are given in units of channels (4 MHz) and integrations (5 ms).

3.3. Temporal, Energy, and Brightness Distributions of Bursts

The burst rate for FRB 121102 varied dramatically throughout the 2016 observing campaign. In the early 2016 campaign, we observed for 30 hr at 3 GHz and no bursts were detected. In the late 2016 campaign, we observed for 27 hr at 3 GHz and detected nine bursts. Overall, the data quality was uniform and high, so the inhomogeneous burst distribution shows that the burst rate was not uniform.

Assuming that the burst detection probability follows a Poisson distribution, the mean VLA burst rate is

$R_{3\text{ GHz}} = 0.16 \pm 0.05 \text{ hr}^{-1}$ above a fluence of 0.2 Jy ms. The nondetection in the first half of VLA observing limits the FRB rate to $R_{3\text{ GHz}} < 0.1 \text{ hr}^{-1}$ (95% confidence limit). This rate was much higher during the late 2016 campaign, $R_{3\text{ GHz}} = 0.3 \pm 0.1 \text{ hr}^{-1}$. This confirms recent analysis of published bursts from FRB 121102 (Opperman & Pen 2017).

The integrated burst flux density is calculated by integrating the burst spectral model (Table 3) in frequency and time. Some VLA burst spectra seem to be contained by the 2.5–3.5 GHz band and most of them seem to have Gaussian envelopes that are well modeled by the emission within that band. Assuming

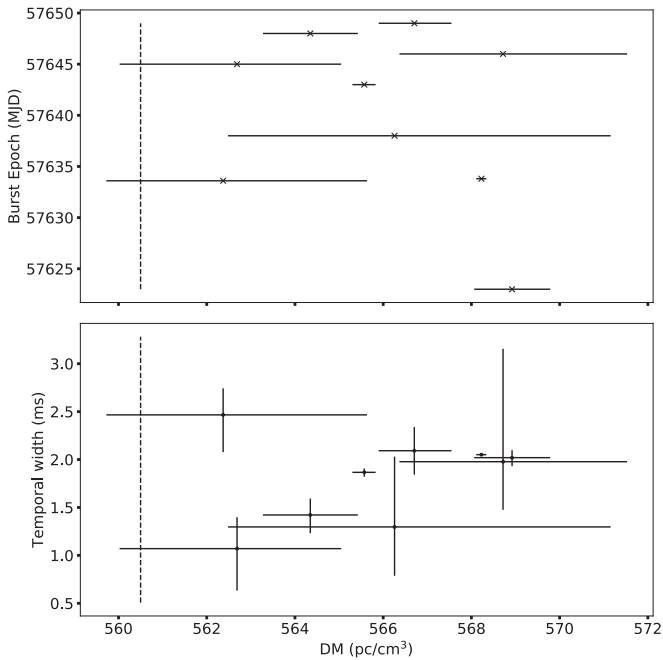


Figure 6. (Top) Burst epoch vs. DM for nine 3 GHz bursts detected by the VLA. The DM scale for both panels is shown at the bottom. The 68% confidence interval on DM is shown with a bar and the dashed line shows the best-fit DM = 560.5 pc cm^{-3} inferred from Arecibo observations at 1.4 GHz (J. W. T. Hessels et al. 2017, in preparation). (Bottom) Temporal width vs. burst DM for the same nine VLA bursts.

that the Gaussian shape defines the full emission window, the integrated 3 GHz flux density can be converted to a total isotropic energy with no further assumptions about the burst spectral properties as

$$E_{\text{int}} = (S_{l,\text{peak}} \times 5 \text{ ms})(2.355\sigma_{\text{ch}} \times 4 \text{ MHz})10^{-23}(4\pi L_d^2) \text{ erg}, \quad (3)$$

where the first term represents the burst fluence, the second term represents the integral of the burst spectrum, 2.355 scales σ to FWHM, and L_d is the luminosity distance to the source.

Figure 7 shows the FRB 121102 burst energy cumulative distribution as seen by the VLA and calculated from prior observations by Arecibo and the Green Bank Telescope (GBT; Scholz et al. 2016; Spitler et al. 2016). The latter two energy distributions are scaled from the fluence by assuming that all burst energy is included by the observation. This likely underestimates the burst energy for some bursts, but should not affect the slope of the distribution. The VLA distribution represents a relatively long campaign, so it is sensitive to lower event rates, but is less sensitive than the single-dish campaigns shown (minimum $E_{\text{int}} \approx 3 \times 10^{38} \text{ erg}$). We also show the rate upper limit (95% confidence) from the early 2016 VLA campaign to demonstrate that even identical observing campaigns have different detection rates.

We modeled the differential energy distribution, $dN/d \log E$, again using a Poisson detection probability with a rate function $\lambda = AE^\alpha$. Rather than trying to estimate a completeness limit for each energy distribution, we assumed an effective detection limit of 0.9 times the weakest burst detected; the best-fit slope is weakly dependent on this, but general conclusions are robust. We directly sampled the likelihood distribution to estimate a best slope of $\alpha_{\text{VLA}} = -0.6^{+0.2}_{-0.3}$, $\alpha_{\text{Arecibo}} = -0.8^{+0.3}_{-0.5}$, and $\alpha_{\text{GBT}} = -0.8^{+0.4}_{-0.5}$

(68% confidence interval). Expressed as a power-law function in dN/dE , the slope index is approximately -1.7 . We caution that propagation effects can potentially modulate the intrinsic flux density and significantly affect any interpretation about burst amplitudes.

4. Discussion

4.1. Burst Spectra

We present the first simultaneous detection of an FRB with multiple telescopes and over frequencies from 1.2 to 3.5 GHz. The flux density of the Arecibo burst detected on MJD 57648 is an order of magnitude less than that seen by the VLA. At the same time, three other bursts from FRB 121102 had similar observing coverage but were not detected simultaneously. This is consistent with the spectral structure observed within the 3 GHz VLA band, which is typically limited to a Gaussian envelope with width of roughly 500 MHz. This confirms earlier results at 1.4 GHz (Scholz et al. 2016; Spitler et al. 2016) with a wider bandwidth and extends the existence of this phenomenon to 3 GHz.

If FRB 121102 burst spectra are typical of the larger FRB population, then population models need to be generalized beyond the assumption of a spectral power law. Most obviously, FRB 121102 implies that future multi-telescope searches for bursts are unlikely to simultaneously detect bursts in different bands (see Sallmen et al. 1999). Second, since burst spectra have limited envelopes, the burst detection rate at one frequency may not represent that at another. Rate estimates for the FRB population will need to explicitly account for the frequency-dependent rate. Finally, we note that the odds of detecting a burst will improve with bandwidth beyond the gain in sensitivity, since bandwidths wider than the FRB characteristic width are more likely to cover the burst envelope. However, to benefit from this effect, FRB search algorithms will need to search for bursts with spectral width less than the full bandwidth.

After correcting for barycentric and dispersion delays, the VLA+AO burst spectrum has a residual temporal drift. This drift can be interpreted as dispersion in excess of the nominal value inferred from contemporaneous observations at 1.4 GHz (560.5 pc cm^{-3} ; J. W. T. Hessels et al. 2017, in preparation). However, the VLA+AO burst is not the only one with an apparent excess DM; most burst DM measurements are inconsistent with the nominal DM (Figure 6). The scale of this excess DM is comparable to the burst-to-burst variation in DM within the whole sample of VLA 3 GHz bursts. This variation had been noted in earlier 1.4 GHz Arecibo observations of FRB 121102 (Scholz et al. 2016; Spitler et al. 2016), but the VLA bursts demonstrate that this burst-specific DM is seen simultaneously from 1.4 to 3 GHz.

One interpretation for the burst-dependent DM is that the bursts have a frequency-dependent pulse shape. Pulsar pulse shapes evolve with frequency on GHz frequency scales, presumably due to changes in the pulsar beam shape (Lyne & Manchester 1988). The burst-dependent DM changes are on the order of 1% of the total DM (equivalent to a delay rate up to 2 ms GHz^{-1}), which is much larger than typically observed for pulsars (Lentati et al. 2017).

Another possibility is that there is intrinsic structure to the pulses from FRB 121102. Figure 5 shows how the spectro-temporal distribution of one burst was not well modeled by a

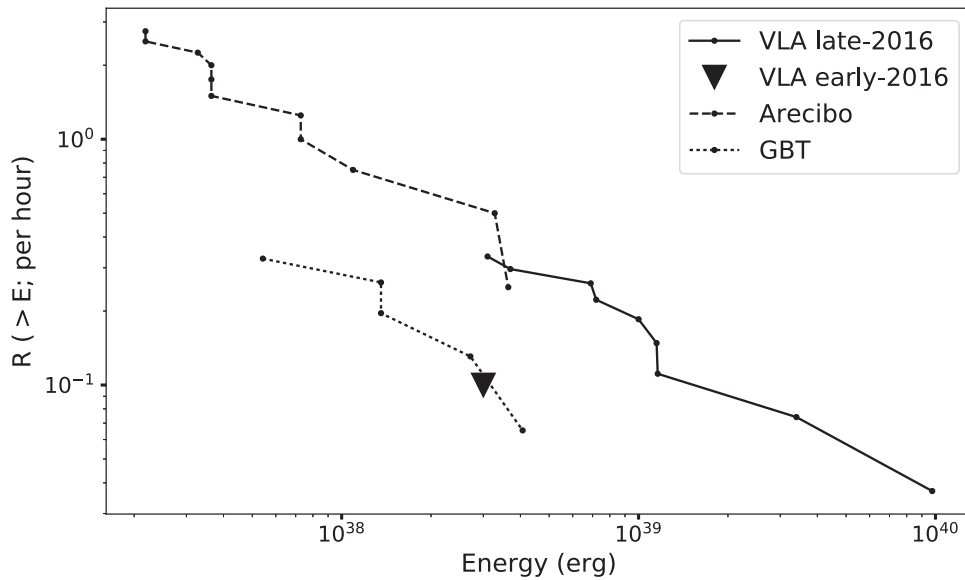


Figure 7. Cumulative burst isotropic energy distributions for the VLA, Arecibo, and GBT bursts are shown with dots connected by solid, dashed, and dotted lines, respectively. The Arecibo distribution is derived from the 11 1.4 GHz bursts reported in Spitler et al. (2016) and the GBT distribution is derived from the 5 1.4 GHz bursts reported in Scholz et al. (2016). An upper limit from the VLA nondetection in early 2016 is shown as a triangle.

single component. This is consistent with more complex burst structure seen toward FRB 121102 and other FRBs (Champion et al. 2016; Spitler et al. 2016). Our modeling of the VLA burst dynamic spectra show a weak correlation between larger apparent DM and pulse width. This could be a signature of unresolved spectrotemporal structure in the VLA burst spectra that biases the measured DM. If so, then the systematic measurement of higher DMs by the VLA ($\sim 5 \text{ pc cm}^{-3}$ higher than nominal) requires that the intrinsic structure evolve toward lower frequencies during the burst.

The burst-specific DM structure could be intrinsic to the emission mechanism or induced during propagation. Radio waves can be modified in a variety of ways (e.g., scintillation, scattering) and the duration of the emission in the source frame is not known (Cordes et al. 2016). Cordes et al. (2017) describe a model where plasma lensing near the source of an FRB can magnify radio emission by orders of magnitude. Plasma lensing can also produce multiple burst images separated by timescales from microseconds to tens of milliseconds or longer. These burst images would also have slightly different DMs. Lensing amplifications have a complicated frequency dependence that includes spikes, plateaus, and troughs. The simultaneous detection of burst MJD 57648 with both Arecibo (L band) and the VLA (S band up to 3.2 GHz) requires a focal frequency $\gtrsim 3.2$ GHz and sufficient amplification in both bands.

4.2. Energy Distribution

Our refined analysis shows that FRB 121102 has isotropic energies as high as $E_{\text{max}} \approx 10^{40}$ erg. While this emission is coherent and beamed, the apparent energy is larger than Galactic analogues such as the giant pulses from the Crab pulsar ($\sim 10^{35}$ erg, $T_{b,\text{Crab}} \sim 10^{41}$ K; Hankins et al. 2003; Katz 2014). Radio bursts from FRB 121102 require either dramatic scaling of known emission processes (Cordes & Wasserman 2016; Lyutikov et al. 2016) and/or strong amplification by propagation effects (Cordes et al. 2017).

In Section 3.3 we compare the energy distribution of the nine VLA bursts to those reported earlier by Arecibo and the GBT.

All three energy distributions can be characterized as a power law in dN/dE with slope ~ -1.7 . This slope is seen even though the burst rate varies by almost an order of magnitude between campaigns and the observing frequencies cover both 1.4 and 3 GHz bands. This suggests that the slope is related to the underlying physical process, rather than the burst detection rate at any given time. The value of the energy distribution slope is similar to that derived from high-energy bursts from magnetars (Göğüş et al. 2000; Scholz & Kaspi 2011), which may be examples of self-regulated critical phenomena (slope = $-5/3$; Aschwanden 2011). This is consistent with the idea that magnetar bursts can generate both the millisecond-duration bursts and persistent radio emission from FRB 121102 (Beloborodov 2017).

4.3. Flux Distribution

New FRB discoveries have often surprised observers with their remarkable brightness (Lorimer et al. 2007; Ravi et al. 2016). When modeling the flux distribution as a power law, a uniform, isotropic distribution of sources will have a power-law index, α , of -1.5 . Prior to the measurement of the first GRB redshift, deviations from this Euclidean distribution were used to infer their cosmological distribution (e.g., the V/V_{max} test; Mao & Paczynski 1992; Fenimore & Bloom 1995). Multiple studies have suggested that FRBs have a sub-Euclidean flux distribution ($-0.5 < \alpha < -0.9$; Vedantham et al. 2016; Lawrence et al. 2017; Li et al. 2017). Others have noted that the flux distribution is not well modeled as a power law, such that α is effectively sensitivity (and telescope) dependent (Oppermann et al. 2016; CHIME Scientific Collaboration et al. 2017).

We now know that FRB 121102 would be detectable with the VLA out to $z=0.7$, which suggests that cosmological effects are even more important for understanding properties of the FRB population. CHIME Scientific Collaboration et al. (2017) demonstrate how redshift space distortions, time dilation, and spectral index (“k-correction”) effects can flatten the flux distribution. To this complex scene, we add the fact

that FRB 121102 burst spectra are not defined by a spectral index, which suggests that k-corrections are likely to be very difficult to calculate in practice. If the FRB burst rate is higher at low (rest) radio frequencies, then high-redshift FRBs will have a lower (redshifted) rate that flattens the dN/dF distribution in a manner similar to a k-correction. However, propagation effects are expected to suppress the FRB rate at sub-GHz frequencies (Chawla et al. 2017; Rajwade & Lorimer 2017) as well. The VLA and Arecibo observed intensively in a coordinated fashion during the late 2016 campaign and a comparison of their relative rates will be presented elsewhere.

4.4. Repetition

The chance of detecting a burst from FRB 121102 with the VLA changes substantially on day-to-month timescales. A major outstanding question is whether this time-variable rate is driven by an intrinsic process (Katz 2016) or extrinsic (propagation) effects in the host galaxy or intergalactic medium (Cordes et al. 2017). However, the temporal distribution of VLA detections alone shows that the FRB 121102 burst rate is significantly correlated on short timescales. That is, detecting a burst implies a higher likelihood of detecting another burst soon thereafter, and not detecting a burst also implies a higher likelihood of not detecting another burst soon thereafter.

If FRB 121102 is representative of the larger FRB population, then recent modeling of their temporal distribution as a “red spectrum” (Connor et al. 2016a) or a modified Poisson distribution (Opperman & Pen 2017) will be important to interpreting survey results. Both temporal models imply that existing observational constraints on repetition are weaker than expected from Poissonian statistics (Petroff et al. 2015; Law et al. 2015). If the clustered bursts are typical of the FRB population, then wide, shallow surveys are the preferred strategy for blind detection of FRBs. Also, since “bursts predict bursts,” many short observations are more likely to detect an FRB than a single long observation of the same total length and all new FRB detections should be immediately and intensively followed up.

4.5. Volumetric Rate of FRB Sources

Thornton et al. (2013) estimated an isotropic rate of FRB events of 10^{-3} galaxy $^{-1}$ yr $^{-1}$ by calculating the number of Milky Way-type galaxies out to a distance implied by assuming all extragalactic DM originates in the intergalactic medium ($z \approx 0.9$ for $DM \approx z \times 900$ pc cm $^{-3}$; Ioka 2003; Inoue 2004). This rate is high (comparable to the rate of core-collapse supernovae; Diehl et al. 2006), which has been used to argue that FRBs are likely not associated with other classes of transient, such as LGRBs or rare subclasses of supernovae (Woosley & Bloom 2006). However, since this rate depends on telescope sensitivity, it is not appropriate to compare to other estimates based on source counts.

Here, we re-evaluate the FRB volumetric rate by assuming FRB 121102 is a prototype of the class and recasting it as a volumetric rate of FRB sources (i.e., a birth rate). Crudely, the volumetric rate of FRB sources can be defined as $R_{\text{FRB}} = R_p / (N_r \Omega_b V(z))$, where R_p is the projected FRB rate, N_r is the number of bursts per source in a typical lifetime, Ω_b is the beaming fraction, and $V(z)$ is the comoving volume out to redshift z . The latest estimates of the projected FRB rate are 2×10^3 sky $^{-1}$ day $^{-1}$ at high Galactic latitudes and flux

densities brighter than 1 Jy ms (Champion et al. 2016; Rane et al. 2016; Lawrence et al. 2017). There is little constraint on the beaming factor, but Galactic pulsars have beaming solid angle fractions on the order of 10% (Tauris & Manchester 1998).

FRB 121102 has an absolute energy scale that can be used to estimate a horizon scale for the typical FRB survey sensitivity. At the typical Parkes survey parameters (e.g., Champion et al. 2016), a survey with a fluence limit of 1 Jy ms can detect the brightest burst from FRB 121102 at $z \approx 1$ (i.e., for isotropic energy of $\approx 10^{40}$ erg). The distance inferred from the largest DMs observed (~ 1500 pc cm $^{-3}$; Champion et al. 2016) is somewhat higher, but that likely overestimates distance since DM is expected to have significant contributions from the host galaxy and intervening galaxies (McQuinn 2014; Tendulkar et al. 2017).

Using an assumed horizon redshift of 1, we estimate a rate of $R_{\text{FRB}} \approx 5 \times 10^{-5} N_r^{-1} (0.1/\Omega_b)$ Mpc $^{-3}$ yr $^{-1}$. This calculation ignores time dilation, which underestimates the burst rate by a factor of 2 at the redshift horizon. The narrow burst spectral structure seen for FRB 121102 also suggests that the FRB rate is understated by a factor of a few by ignoring bursts that fall outside the observing band. Finally, we note that this estimate assumes that Galactic latitude and propagation effects do not significantly affect the detectability of FRBs, although scintillation and scattering likely play significant roles (Macquart & Johnston 2015; Cordes et al. 2017).

Despite its many assumptions, this volumetric birth rate is more appropriate for comparison to rates used for other classes of transient. The LGRB and SLSN-I rates are 10^{-7} and 10^{-8} Mpc $^{-3}$ yr $^{-1}$, respectively (Guetta & Della Valle 2007; Gal-Yam 2012). Comparing the FRB rate to these rates implies that FRB-emitting sources can be generated in LGRBs and SLSN-I if FRBs repeat 5×10^2 and 5×10^3 times. This is consistent with a related rate comparison presented in Nicholl et al. (2017). Here, we have assumed isotropic burst energies of $\sim 10^{40}$ erg or intrinsic energies of $\sim 10^{39} (\Omega_b/0.1)$ erg.

Metzger et al. (2017) use the young magnetar model for FRBs to calculate the maximum number of bursts that can be powered by its magnetic field as $\approx 3000 (0.1/\Omega_b)$ for an isotropic energy of 10^{40} erg. This rate comparison suggests that the SLSN-I rate is most consistent with the FRB rate, although there is significant room for adjustment in the models and rate estimate. The VLA observations of FRB 121102 imply that roughly 200 bursts of this energy were emitted during the month of peak activity. This suggests that FRB 121102 data could be in tension with the young magnetar model, if this level of activity were sustained for roughly a year.

5. Conclusions

The recent precision localization of FRB 121102 has helped identify a host galaxy, measure its distance, and establish it as a member of a truly new class of astrophysical sources. With its cosmological distance firmly established and a rich data set of many bursts, FRB 121102 serves as a prototype that can be used to infer properties of the larger FRB population.

We presented the first multi-telescope detection (Arecibo and VLA) of an FRB. By detecting this burst from 1.2 to 3.5 GHz, we have demonstrated that some bursts have broad spectral structure. However, the energy of that burst was dominated by the VLA 3 GHz observing band and three other VLA bursts are undetected by simultaneous observations at other telescopes.

This demonstrates the burst spectra are poorly described by a power law with a single spectral index. We also modeled dynamic spectra within the VLA 3 GHz band and showed that most bursts can be characterized by a Gaussian envelope of width ~ 500 MHz. This modeling also shows that the apparent DM changes from burst to burst and that DM is biased above the long-term average measured at 1.4 GHz. The nature of this DM change is not known, but could be explained by strong frequency-dependent profile evolution or unresolved spectro-temporal structure in the bursts.

With a characteristic burst spectrum, we can estimate total isotropic radio energy per burst. The cumulative energy distribution is characterized by a power law in dN/dE with slope of ~ -1.7 . The amplitude of this power law changes significantly between observational campaigns. The stochastic nature of the burst rate suggests that past constraints on FRB repetition are weaker than previously inferred. The relatively narrow spectral structure, flat energy distribution, and variable burst rate of FRB 121102 suggests that repeated observations, wide bandwidth, and large instantaneous field of view all improve the odds of FRB discovery.

Assuming that FRB 121102 is representative of the FRB population, we calculate a volumetric birth rate of FRB sources that does not depend on telescope sensitivity. We estimate a volumetric rate of FRB sources of $R_{\text{FRB}} \approx 5 \times 10^{-5} (0.1/\Omega_b) \text{ Mpc}^{-3} \text{ yr}^{-1}$, which is appropriate for FRB 121102-like isotropic burst energies of 10^{40} erg that are detectable out to $z = 1$. This rate is broadly consistent with models of FRBs from young pulsars or magnetars born in SLSN-I or LGRBs, if the typical FRB repeats on the order of 10^3 times over its lifetime. However, if FRB 121102 continues to produce energetic bursts at a high rate, this may argue that extrinsic effects amplify the bursts (Cordes et al. 2017).

New, arcsecond-scale localizations will be critical to refining the picture presented here and constraining models of FRB origin. FRB 121102 was localized within hours by a prototype version of *realfast* and an expanded *realfast* system is now under construction. This platform will search a TB/hr data stream in real time in parallel with ongoing VLA observations, potentially detecting and localizing multiple FRBs per year.

We thank the VLA staff for their support of *realfast* development and Liam Connor for useful feedback. We acknowledge partial support from the Research Corporation for Scientific Advancement (RCSA) for participation in the meeting Fast Radio Bursts: New Probes of Fundamental Physics and Cosmology at the Aspen Center for Physics (February 12-17, 2017).
















The National Radio Astronomy Observatory is a facility of the National Science Foundation operated under cooperative agreement by Associated Universities, Inc.. Part of this research was carried out at the Jet Propulsion Laboratory, California Institute of Technology, under a contract with the National Aeronautics and Space Administration. This research made use of Astropy, a community-developed core Python package for Astronomy (Astropy Collaboration et al. 2013). C.J.L. is supported by the University of California Office of the President under Lab Fees Research Program Award 237863 and NSF award 1611606. MAM is supported by NSF award 1458952. J.W.T.H., C.G.B., and D.M. acknowledge support from the European Research Council under the European Union's Seventh Framework

Programme (FP/2007-2013)/ERC Grant Agreement nr. 337062 (DRAGNET; PI Hessels). J.W.T.H. also acknowledges funding from an NWO Vidi fellowship. S.P.T. acknowledges support from the McGill Astrophysics Fellowship. K.P.M.'s research is supported by the Oxford Centre for Astrophysical Surveys which is funded through the Hintze Family Charitable Foundation. A.S. gratefully acknowledges support from the European Research Council under grant ERC-2012- StG-307215 LODESTONE. The AMI-LA telescope gratefully acknowledges support from the European Research Council under grant ERC-2012- StG-307215 LODESTONE, the UK Science and Technology Facilities Council (STFC) and the University of Cambridge. P.S. holds a Covington Fellowship at DRAO. M.W.A. was a participant in the 2016 Research Experience for Undergraduates in Astronomy and Astrophysics at Cornell University program, supported by grant NSF/AST-1156780. The LWA1 station is supported by the National Science Foundation under grant 1139974 of the University Radio Observatory program. V.M.K. acknowledges support from NSERC, CIFAR, the Canada Research Chair Program and from the Lorne Trottier Chair in Astrophysics & Cosmology.

Facilities: EVLA, Arecibo, Effelsberg, LWA, AMI.

Software: *rtpipe* (Law 2017), *realfast*, *pwkit* (Williams et al. 2017), *emcee* (Foreman-Mackey et al. 2013).

ORCID iDs

C. J. Law  <https://orcid.org/0000-0002-4119-9963>
 G. C. Bower  <https://orcid.org/0000-0003-4056-9982>
 S. Burke-Spolaor  <https://orcid.org/0000-0003-4052-7838>
 S. H. Carey  <https://orcid.org/0000-0002-0221-6871>
 J. M. Cordes  <https://orcid.org/0000-0002-4049-1882>
 K. Grainge  <https://orcid.org/0000-0002-6780-1406>
 J. W. T. Hessels  <https://orcid.org/0000-0003-2317-1446>
 V. M. Kaspi  <https://orcid.org/0000-0001-9345-0307>
 M. A. McLaughlin  <https://orcid.org/0000-0001-7697-7422>
 K. Mooley  <https://orcid.org/0000-0002-2557-5180>
 Y. C. Perrott  <https://orcid.org/0000-0002-6255-8240>
 S. M. Ransom  <https://orcid.org/0000-0001-5799-9714>
 P. Scholz  <https://orcid.org/0000-0002-7374-7119>
 K. Stovall  <https://orcid.org/0000-0002-7261-594X>
 S. P. Tendulkar  <https://orcid.org/0000-0003-2548-2926>

References

- Aschwanden, M. J. 2011, *SoPh*, **274**, 99
- Astropy Collaboration, Robitaille, T. P., Tollerud, E. J., et al. 2013, *A&A*, **558**, A33
- Beloborodov, A. M. 2017, *ApJL*, **843**, L26
- Champion, D. J., et al. 2016, *MNRAS*, **460**, L30
- Chatterjee, S., et al. 2017, *Natur*, **541**, 58
- Chawla, P., et al. 2017, *ApJ*, **844**, L40
- CHIME Scientific Collaboration, Amiri, M., Bandura, K., et al. 2017, arXiv:1702.08040
- Connor, L., Pen, U.-L., & Oppermann, N. 2016a, *MNRAS*, **458**, L89
- Connor, L., Sievers, J., & Pen, U.-L. 2016b, *MNRAS*, **458**, L19
- Cordes, J. M., & Lazio, T. J. W. 2002, arXiv:astro-ph/0207156
- Cordes, J. M., & Wasserman, I. 2016, *MNRAS*, **457**, 232
- Cordes, J. M., Wasserman, I., Hessels, J. W. T., et al. 2017, *ApJ*, **842**, 35
- Cordes, J. M., Wharton, R. S., Spitler, L. G., Chatterjee, S., & Wasserman, I. 2016, arXiv:1605.05890
- Cordes, J. M., et al. 2006, *ApJ*, **637**, 446
- Diehl, R., et al. 2006, *Natur*, **439**, 45
- Dokuchaev, V. I., & Eroshenko, Y. N. 2017, arXiv:1701.02492
- DuPlain, R., Ransom, S., Demorest, P., et al. 2008, *Proc. SPIE*, **7018**, 70191D

- Ellingson, S. W., et al. 2013, *ITAP*, **61**, 2540
- Fenimore, E. E., & Bloom, J. S. 1995, *ApJ*, **453**, 25
- Ford, J. M., Demorest, P., & Ransom, S. 2010, *Proc. SPIE*, **7740**, 77400A
- Foreman-Mackey, D. 2016, *JOSS*, **24**
- Foreman-Mackey, D., Hogg, D. W., Lang, D., & Goodman, J. 2013, *PASP*, **125**, 306
- Fuller, J., & Ott, C. D. 2015, *MNRAS*, **450**, L71
- Gal-Yam, A. 2012, *Sci*, **337**, 927
- Goodman, J., & Weare, J. 2010, *Communications in Applied Mathematics and Computational Science*, **5**, 65
- Göğüş, E., Woods, P. M., Kouveliotou, C., et al. 2000, *ApJL*, **532**, L121
- Guetta, D., & Della Valle, M. 2007, *ApJL*, **657**, L73
- Hankins, T. H., Kern, J. S., Weatherall, J. C., & Eilek, J. A. 2003, *Natur*, **422**, 141
- Inoue, S. 2004, *MNRAS*, **348**, 999
- Ioka, K. 2003, *ApJL*, **598**, L79
- Kashiyama, K., & Murase, K. 2017, arXiv:1701.04815
- Katz, J. I. 2014, *PhRvD*, **89**, 103009
- Katz, J. I. 2016, *ApJ*, **826**, 226
- Kulkarni, S. R., Ofek, E. O., Neill, J. D., Zheng, Z., & Juric, M. 2014, *ApJ*, **797**, 70
- Law, C. J. 2017, Rtpipe: Searching for Fast Radio Transients in Interferometric Data, Astrophysics Source Code Library
- Law, C. J., et al. 2015, *ApJ*, **807**, 16
- Lawrence, E., Vander Wiel, S., Law, C. J., Burke Spolaor, S., & Bower, G. C. 2017, *AJ*, **154**, 11
- Lazarus, P., et al. 2015, *ApJ*, **812**, 81
- Lentati, L., et al. 2017, *MNRAS*, **466**, 3706
- Li, L., Huang, Y., Zhang, Z., Li, D., & Li, B. 2017, *RAA*, **17**, 6
- Lorimer, D. R., Bailes, M., McLaughlin, M. A., Narkevic, D. J., & Crawford, F. 2007, *Sci*, **318**, 777
- Lunnan, R., et al. 2014, *ApJ*, **787**, 138
- Lyne, A. G., & Manchester, R. N. 1988, *MNRAS*, **234**, 477
- Lyutikov, M., Burzawa, L., & Popov, S. B. 2016, *MNRAS*, **462**, 941
- Macquart, J.-P., & Johnston, S. 2015, *MNRAS*, **451**, 3278
- Mao, S., & Paczynski, B. 1992, *ApJL*, **388**, L45
- Marcote, B., et al. 2017, *ApJL*, **834**, L8
- McQuinn, M. 2014, *ApJL*, **780**, L33
- Metzger, B. D., Berger, E., & Margalit, B. 2017, arXiv:1701.02370
- Modjaz, M., et al. 2008, *AJ*, **135**, 1136
- Nicholl, M., Williams, P. K. G., Berger, E., et al. 2017, *ApJ*, **843**, 84
- Opperman, N., & Pen, U.-L. 2017, arXiv:1705.04881
- Oppermann, N., Connor, L. D., & Pen, U.-L. 2016, *MNRAS*, **461**, 984
- Perrott, Y. C., et al. 2013, *MNRAS*, **429**, 3330
- Petroff, E., et al. 2015, *MNRAS*, **454**, 457
- Petroff, E., et al. 2016, *PASA*, **33**, e045
- Planck Collaboration, et al. 2016, *A&A*, **594**, A13
- Popov, S. B., & Pshirkov, M. S. 2016, *MNRAS*, **462**, L16
- Rajwade, K. M., & Lorimer, D. R. 2017, *MNRAS*, **465**, 2286
- Rane, A., Lorimer, D. R., Bates, S. D., et al. 2016, *MNRAS*, **455**, 2207
- Ransom, S. M. 2001, PhD thesis, Harvard Univ.
- Ravi, V., Shannon, R. M., Bailes, M., et al. 2016, *Sci*, **354**, 1249
- Sallmen, S., Backer, D. C., Hankins, T. H., Moffett, D., & Lundgren, S. 1999, *ApJ*, **517**, 460
- Scholz, P., & Kaspi, V. M. 2011, *ApJ*, **739**, 94
- Scholz, P., Spitler, L. G., Hessels, J. W. T., et al. 2016, *ApJ*, **833**, 177
- Spitler, L. G., et al. 2014, *ApJ*, **790**, 101
- Spitler, L. G., et al. 2016, *Natur*, **531**, 202
- Tauris, T. M., & Manchester, R. N. 1998, *MNRAS*, **298**, 625
- Tendulkar, S. P., et al. 2017, *ApJL*, **834**, L7
- Thompson, C. 2017, *ApJ*, **844**, 162
- Thornton, D., et al. 2013, *Sci*, **341**, 53
- Vedantham, H. K., Ravi, V., Hallinan, G., & Shannon, R. M. 2016, *ApJ*, **830**, 75
- Williams, P. K. G., Clavel, M., Newton, E., & Ryzhkov, D. 2017, Pwkit: Astronomical Utilities in Python, Astrophysics Source Code Library, <https://ascl.net/1704.001>
- Woosley, S. E., & Bloom, J. S. 2006, *ARA&A*, **44**, 507
- Zhang, B. 2017, arXiv:1701.04094
- Zwart, J. T. L., et al. 2008, *MNRAS*, **391**, 1545